Liquid chromatography-quadrupole time-of-flight mass spectrometry for screening in vitro drug metabolites in humans : investigation on seven phenethylamine-based designer drugs

Liquid chromatography-quadrupole time-of-flight mass spectrometry for screening *in vitro* drug metabolites in humans: investigation on seven phenethylamine-based designer drugs

Foon Yin Lai[a,*], Claudio Erratico[b], Juliet Kinyua[b], Jochen F. Mueller[a], Adrian Covaci[b,*], Alexander L.N. van Nuijs[b]

a. The University of Queensland, The National Research Centre for Environmental Toxicology, 39 Kessels Road, Coopers Plains, QLD 4108, Australia

b. Toxicological Center, University of Antwerp, Universiteitsplein 1, 2610 Antwerp, Belgium

[*]Corresponding authors' details:

Dr. Foon Yin Lai: The University of Queensland, The National Research Centre for Environmental Toxicology (Entox), 39 Kessels Road, Coopers Plains, QLD 4108, Australia.

Tel.: +61 (0)4 06714601; Fax.: +61 (0)7 3274 9003; E-mail: foon.lai@uqconnect.edu.au

Prof. Dr. Adrian Covaci: Toxicological Center, Universiteit Antwerpen, Universiteitsplein 1, 2610 Wilrijk-Antwerpen, Belgium.

Tel.: +32 3 265 24 98; E-mail: adrian.covaci@uantwerpen.be

Abstract

Phenethylamine-based designer drugs are prevalent within the new psychoactive substance market. Characterisation of their metabolites is important in order to identify suitable biomarkers which can be used for better monitoring their consumption. Careful design of *in vitro* metabolism experiments using subcellular liver fractions will assist in obtaining reliable outcomes for such purposes. The objective of this study was to stepwise investigate the *in vitro* human metabolism of seven phenethylamine-based designer drugs using individual families of enzymes. This included *para*-methoxyamphetamine, *para*-methoxy-methamphetamine, 4-methylthioamphetamine, *N*-methyl-benzodioxolylbutanamine, benzodioxolyl-butanamine, 5-(2-aminopropyl)benzofuran and 6-(2-aminopropyl)benzofuran. Identification and structural elucidation of the metabolites was performed using liquid chromatography-quadrupole-time-of-flight mass spectrometry. The targeted drugs were mainly metabolised by cytochrome P450 enzymes via *O*-dealkylation as the major pathway, followed by *N*-dealkylation, oxidation of unsubstituted C atoms and deamination (to a small extent). These drugs were largely free from Phase II metabolism. Only a limited number of metabolites were found which was consistent with the existing literature for other phenethylamine-based drugs. Also, the metabolism of most of the targeted drugs progressed at slow rate. The reproducibility of the identified metabolites was assessed through examining formation patterns using different incubation times, substrate and enzyme concentrations. Completion of the work has led to a set of metabolites which are representative for specific detection of these drugs in intoxicated individuals and also for meaningful evaluation of their use in communities by wastewater-based drug epidemiology.

Keywords: new psychoactive substances, metabolite characterisation, high-resolution mass spectrometry, wastewater-based epidemiology, LC-QTOF-MS analysis

Introduction

In recent years, there has been a clear increasing trend in the production and use of new psychoactive substances (NPS), internationally [1]. NPS are considered as substances that are not under the control of the 1961 Single Convention on Narcotic Drugs or the 1971 Convention on Psychotropic Substances but which may pose a threat to public health [1-3]. There are many different families of NPS, such as phenethylamines, cathinones, piperazines, and synthetic cannabinoids [2]. In the global NPS market, the number of phenethylamine derivatives was ranked as the second highest and accounted for about 23% of the total number of reported NPS in 2009–2012 [2]. To circumvent legislative band, these phenethylamine-based designer drugs are typically chemically modified from the molecular structure of classical phenethylamine-based illicit drugs, such as amphetamines and 3,4-methylenedioxymethamphetamine (MDMA), and still maintain amphetamine- and/or MDMA-like physiological effects. The description of a substance as an NPS does not necessarily mean it is an entirely novel substance, but can also reflect recent increased availability on the drug market [1-3]. For instance, *para*-methoxymethamphetamine (PMMA), first synthesised in the late 1930s, emerged on the drug market in 2011-2013 and then appeared again recently causing several fatal intoxication cases in England, the Netherlands and Australia [4-6].

Identification of NPS and their specific metabolites in human samples (e.g. serum, urine and/or saliva) is critical in forensic and clinical toxicology for provision of intoxication evidence. Also, research related to determining NPS metabolites is beneficial to the emerging field of wastewater-based drug epidemiology, in which specific drug metabolites are measured in wastewater to back-estimate the use of these substances in communities [7, 8]. A few recent studies have analysed raw wastewater samples for some phenethylamine-based designer drugs to understand their use in the communities [9-13]. Monitoring metabolised drug residues in addition to the parent drug could improve efforts to determine the extent of

74 the population use of these substances, especially when the parent drug concentrations in
75 wastewater are low or below the sensitivity of analytical methods.

76 Due to the ethical limitation on studying *in vivo* drug metabolism in humans, an *in vitro*
77 approach has been proposed to offer a relatively efficient and direct alternative [14]. The
78 approach usually involves: (a) incubation of the NPS of interest with pooled human liver
79 microsomes (HLM) for an overview of metabolism (rather than particular types of
80 isoenzymes to understand specific metabolic processes); (b) using high resolution mass
81 spectrometry (HRMS) to screen for all metabolites of the selected NPS; (c) elucidation of the
82 structure of individual metabolites based on its accurate mass, MS/MS fragmentation,
83 isotopic patterns and values of double bond equivalent. Liquid chromatography (LC)
84 combined with HRMS such as quadrupole-time-of-flight MS (QTOF-MS) has been
85 recognised as one of the most robust and widely applied techniques for identifying drug
86 metabolites in *in vivo* and *in vitro* matrices, facilitating discovery of NPS metabolites [15,
87 16]. Together, LC-HRMS with careful *in vitro* experimental designs such as using multiple
88 incubation time points, repeating the experiments and/or using individual enzyme families to
89 assess specific (groups of) metabolites, the reliability of the *in vitro* metabolism data can be
90 enhanced.

91 This study selected seven phenethylamine-based designer drugs, including *para*-
92 methoxyamphetamine (PMA), PMMA, 4-methylthioamphetamine (4-MTA), *N*-methyl-
93 benzodioxolylbutanamine (MBDB), benzodioxolylbutanamine (BDB), 5-(2-
94 aminopropyl)benzofuran (5-APB) and 6-(2-aminopropyl)benzofuran (6-APB) (Fig. 1) to
95 assess its human *in vitro* metabolism. These drugs are commonly considered as NPS, except
96 for PMA and 4-MTA which were listed on the 1971 Convention on Psychotropic Substances
97 as of September 2013. Also, a few of them including MBDB, 4-MTA and PMMA have been
98 included in the Risk Assessment Reports of the European Monitoring Centre for Drugs and
99 Drug Addiction [17]. The rationale for this study is based on the fact that there is a lack of a

clear understanding of human *in vitro* metabolites for these drugs; as previous related *in vitro* studies have been limited to a focus on understanding what types of isoenzymes participate in specific metabolism processes [18-23], and also that there have been no studies performed for the screening and structural elucidation of potential *in vitro* metabolites of these drugs using LC-HRMS. Furthermore, no comparisons of human *in vitro* metabolism for these drugs, which are closely related in structure, have ever been made under the same experimental conditions.

Therefore, the main objective of this study was to screen for potential *in vitro* metabolites of these designer drugs to be formed in HLM using untargeted analysis with LC-QTOF-MS. Hence, HLM as an enzyme cocktail was applied, instead of selected types of isoenzymes [18-23], to generate all the possible cytochrome P450 metabolites. Also, this study aimed to assess the *in vitro* metabolism of these drugs in a stepwise experimental design with individual enzyme family preparations, and to characterise their potential metabolites, propose and compare their respective metabolic pathways.

1. Materials and methods

1.1. Chemicals and reagents

Chemical standards for PMA, PMMA, 4-MTA, MBDB, BDB, 5-APB and 6-APB were obtained from LGC Standards SARL (Molsheim, France) and Cerilliant (Round Rock, Texas, USA) at the concentration of 1 mg/mL in methanol or acetonitrile. The internal standard, theophylline, was obtained as powder (anhydrous, purity>99%) from Sigma-Aldrich (Diegem, Belgium). Pooled human liver microsomes (HLM; mix gender, n=50) were purchased from Tebu-bio (Boechout, Belgium). Pooled human liver cytosol (HLCYT; mix gender, n=50), chemical standards for 2,6-uridinediphosphate glucuronic acid (UDPGA), alamethicin (neat, purity>99%), 3'-phosphoadenosine-5'-phosphosulfate (PAPS; neat, purity>60%) lithium salt hydrate, 4-nitrophenol (4-NP), 4-nitrophenol-glucuronide (4-NP-

Gluc; neat, purity>99%), 4-nitrophenol-sulfate (4-NP-Sulf; neat, purity>99%), naphthol-glucuronide (Naphth-Gluc; neat, purity>99%), 5-bromo-4-chloro-3-indolyl sulfate (Indolyl-Sulf; neat, purity>99%) and NADPH (neat, purity>99%) were purchased from Sigma-Aldrich (Diegem, Belgium). Ultrapure water was prepared using a Purelab flex water system by Elga (Tienen, Belgium). Acetonitrile, methanol, ammonium hydroxide, hydrochloric acid and ammonium acetate were purchased from Merck (Darmstadt, Germany). All organic solvents were HPLC grade or higher.

1.2. Tiered approaches on *in vitro* drug metabolism

In this study, a two-tiered approach for investigating Phase I and Phase II *in vitro* drug metabolism was followed (Fig. 2). The purpose of tier I was to screen for the major metabolites formed and the family of enzymes involved in their formation, in a similar manner to the typical practice for *in vitro* metabolism studies. Tier I consisted of two parts, tier-IA and -IB. In tier IA, a direct metabolism of the drugs of interest was investigated, in which Phase I metabolites and direct Phase II metabolites of the parent drug (when possible to be formed) were screened. This allowed investigation of direct drug metabolism mediated separately by Phase I and Phase II enzymes. After that, tier IB was employed to investigate the Phase II metabolism of Phase I metabolites detected in tier IA, providing information on the formation of secondary metabolites. Tier II aimed to assess the consistency and reproducibility of the metabolite formed in tier I and to determine the major, intermediate and minor metabolites by monitoring over various incubation times (10, 20, 40, 60, and 90 min), enzyme concentrations (0.2, 0.4, 0.6, and 0.8 mg/mL) and substrate concentrations (1, 3, 5, and 10 µM).

1.3. *In vitro* drug metabolism assays

For tier IA samples focusing on cytochrome P450 (CYP) enzymes, the reaction mixture (final volume: 1 mL), consisting of 100 mM phosphate buffer (pH 7.4), HLM (final concentration: 0.5 mg/mL) and the substrate (final concentration: 10 µM) was pre-incubated

for 5 min in a shaking water bath at 37 °C. The reaction was initiated by addition of 10 µL of NADPH solution (final concentration: 1 mM) in the phosphate buffer. To keep the NADPH concentration saturated, an extra aliquot was added every hour. To stop the reaction after 2 h, 250 µL of an ice-cold acetonitrile solution containing 1% formic acid and 5.0 µg/mL of theophylline (used as internal standard) was added to each sample, which was then vortex-mixed for 30 s and centrifuged at 8,000 rpm for 5 min. The supernatant was then transferred to a glass tube, and concentrated to 200 µL under a gentle stream of nitrogen gas at 60 °C. A 20 µL aliquot of acetonitrile was then added to the extract before transferring it to a HPLC vial for analysis. For tier IA samples focusing on uridinediphosphate glucuronic acid transferase (UGT) enzymes, the reaction mixture was prepared as described above for CYP enzyme samples, but adding a 10 µL aliquot (final concentration: 10 µg/mL) of alamethicin (for opening the pore of microsomal inner lumen, where UGTs are expressed) dissolved in dimethyl sulfoxide before pre-incubating the samples in the water bath. Also, the cofactor UDPGA was used instead of NADPH, but at the same final concentration (1 mM). An aliquot of UDPGA was added to the reaction mixture every hour, similarly to NADPH in the CYP experiments. In tier IA samples focusing on sulfotransferase (SULT) enzymes, the reaction mixture was prepared as described above for CYP enzyme samples, but using HLCYT (final concentration: 0.5 mg/mL) instead of HLM and using PAPS instead of NADPH as the cofactor at the same final concentration (1 mM). An aliquot of PAPS was added to the reaction mixture every hour. Samples were then processed as described above for CYP enzyme samples.

In tier IB, formation of glucuronidated and sulfated metabolites of the Phase I metabolites produced in tier IA experiments was investigated in two major steps. First, Phase I metabolites of the drug of interest were enzymatically produced as described in tier IA for three hours. The reaction was quenched by keeping the samples on ice for 5 min, followed by centrifugation at 8,000 rpm for 5 min. Then, 940 µL of the supernatant, containing the

fraction of parent drug and its metabolites generated by CYP enzymes, was transferred to a new tube which contained a fresh aliquot of pooled HLM or HLCYT (final concentration: 0.5 mg/mL) for the samples investigating UGT or SULT mediated metabolism, respectively. Alamethicin and the appropriate cofactors were added at the concentrations and time intervals described above for tier IA samples. The samples were incubated for two hours and prepared as described above.

In the tier II experiments, three different sets of samples were prepared. In the first set, the reaction mixture (1 mL) consisted of 100 mM phosphate buffer, pooled HLM (0.8 mg/mL) and the substrate (10 µM). The reaction was initiated by addition of NADPH, and stopped after 10, 20, 40, 60, and 90 min. In the second set, the reaction mixture consisted of 100 mM phosphate buffer, pooled HLM at different total protein concentrations (final concentrations: 0.2, 0.4, 0.6, and 0.8 mg/mL) and a constant concentration of the substrate (10 µM). The reaction was initiated by addition of NADPH and was stopped after 90 min. In the third set, the reaction mixture consisted of 100 mM phosphate buffer, pooled HLM at a constant protein concentration (0.8 mg/mL) and the substrate at different concentrations (final concentrations: 1, 3, 5, and 10 µM). The reaction was initiated by addition of NADPH and was stopped after 90 min. The reaction was quenched and the samples were prepared as described in tier IA section above.

Positive and negative control samples for each family of enzymes of interest were routinely prepared. In the positive control samples for UGT and SULT activity, 4-nitrophenol was selected as the substrate and the formation of 4-nitrophenol-sulfate and 4-nitrophenol-glucuronide, respectively, was monitored. Samples were prepared as described in the tier IA section above. No positive control samples for CYP activity were prepared, because data about the catalytic activity of major human liver CYPs was provided by the HLM vendor. Three different negative control samples were prepared by omitting the enzymes, the

substrate, or the cofactor in the reaction mixture. The negative control samples for CYP, UGT and SULT activity were prepared as described in tier I section above.

1.4. LC-QTOF-MS analysis

Samples were analysed by a LC-QTOF-MS system which consisted of a 1290 Infinity LC (Agilent Technologies) connected to a 6530 Accurate-Mass QTOF-MS (Agilent Technologies). Chromatographic separation of the extracts was achieved using a C_8 Zorbax Eclipse Plus column (150 X 2.1 mm, 3.5 µm, Agilent Technologies) with a mobile phase composition of 5 mM ammonium acetate in ultrapure water (A) and acetonitrile (B) at 40°C. The gradient program was as follows: 2% B for the first 5 min followed by linear increase of B from 2 to 22% from 5 to 25 min and from 22 to 80% from 25 to 26 min. Solvent B was maintained at 80% for 4 min, decreased to 2% from 30 to 30.5 min and kept at 2% from 30 to 40 min to re-equilibrate the column. The total run time was 40 min per sample. The flow rate was 0.2 mL/min with an injection volume of 2 µL.

The acceptable mass accuracy (within ±2 ppm) of the QTOF-MS was calibrated before each analysis using a reference solution for scanning up to 1700 mass-to-charge ratio (*m/z*) with extended dynamic range (2 GHz). Samples were analysed using positive and negative electrospray ionisation (+/-ve ESI) modes individually, with the fragmentor voltage at 300 V and gas temperature 325 °C. The QTOF-MS was set to acquire *m/z* ranging between 50 and 1000 amu at a scan rate of 2.5 spectra per s (i.e. 400 ms/spectrum). The auto-MS/MS function was used to obtain MS/MS spectra of precursor ions using three different collision energies (10, 20 and 40 eV). Precursor ions were targeted if ion abundances exceeded the threshold of 2000 with a maximum of three precursor ions per cycle.. The QTOF-MS was set to scan MS/MS *m/z* from 50 to 500 amu. To avoid over-fragmentation of the same precursor ion, an active exclusion function was set to exclude the precursor ions after every two spectra and release it after 0.2 min. During analysis, the reference mass standard solution (commercially available from Agilent) was constantly infused onto the QTOF-MS for monitoring and

measuring its mass accuracy with the reference masses of 121.0508 and 922.0097 for +ve ESI and of 119.0352 and 980.0152 for -ve ESI.

1.5. Data analysis

Two different approaches were used to assist the interpretation of the potential *in vitro* metabolites formed. For approach 1, potential Phase I metabolites were predicted based on authors' knowledge considering (a) the molecular structure of the drug, (b) the family of enzymes that might be able to metabolise it and (c) the type of reactions that these families of enzymes are known to catalyse. Once the Phase I metabolites were experimentally determined (tier IA experiments), the families of Phase II enzymes that might be able to further metabolise them were identified and the structures of the Phase II metabolites were predicted. For approach 2, possible metabolites were estimated using metabolism-specific software (Nexus v1.5, Lhasa Limited), in which the chemical structure of the drug, the species of interest (i.e. humans), the enzyme families and a minimum likelihood of metabolite formation (i.e. "equivocal") were used for prediction. The prediction was conducted up to tertiary metabolites and for a maximum of 100 metabolites. The two approaches were independently applied to the same acquired raw data file, allowing determinations of their consistency, for better understanding the potential *in vitro* metabolites generated. The approach of data analysis has been previously applied in our team for assessing human *in vitro* metabolism of environmental contaminants [24, 25] and also recently shown feasible for evaluating *in vitro* data on human drug metabolism with *in silico* methods[26].

The chromatographic features of each compound, such as the retention time and peak area counts, were obtained from the extracted ion chromatograms. To confirm the identification of a metabolite, the following criteria were applied: (a) the measured molecular *m/z* of the precursor ion and the product ions should be respectively within 10 and 25 ppm of its theoretical value (higher mass tolerances taken into account lower sensitivities with small amounts of product ions); (b) the isotopic patterns should be overlaid at least 75% with the

predicted ones; (c) the measured double bond equivalent (DBE) value should match with the postulated structure; (d) the absence of the possible metabolite at the same retention time in all the negative control samples; (e) the proposed chemical structure of the detected metabolite has to be logical considering the chemical structure of the substrate and the reactions that the family of enzymes under investigation is able to catalyse; and (f) the retention time of the detected metabolites should not be higher than that of the parent drug. Tier II data are presented as the response value, which was calculated as the peak area ratio of the metabolite or the parent drug to the internal standard (theophylline) for compensating inter-sample and instrumental variability during analysis.

2. Results

2.1. PMA and PMMA

In tier IA samples, the only metabolite of PMA detected was formed via *O*-demethylation catalysed by CYP enzymes, resulting in a *para*-hydroxylated metabolite (PMA-M1) (Table 1 and Fig. 3A). Its molecular ion was *m/z* 152.1063 with the difference in mass error between the measured and theoretical mass (i.e. Δmass) at +4.60 ppm and the measured DBE value at 4 (Table 1). With different collision energy values applied (Fig. S1), the molecular structure of PMA-M1 was elucidated through five potential major fragment ions which were *m/z* 135.0799, 107.0495, 91.0552, 77.0390 and 65.0364 (Table 1, Fig. S1). The fragment ion *m/z* 135.0799 resulted from a loss of NH_3 and then was further fragmented with a loss of C_2H_4 (ethylene) to yield *m/z* 107.0495 ($C_7H_7O^+$). The ion $C_7H_7O^+$ is likely a hydroxyl-tropylium ion which possibly facilitates the loss of the hydroxyl group on the benzyl moiety. The fragment ions *m/z* 91.0552 ($C_7H_7^+$, benzylium ion ↔ tropylium ion), 77.0390 ($C_6H_5^{\bullet+}$, radical benzene) and 65.0364 ($C_5H_5^{\bullet+}$, a loss of CH≡CH from tropylium ion) represent the hallmark features of the alkylbenzene moiety [27]. Also, PMA-M1 eluted approximately 10 min earlier than the parent compound, suggesting that it has a higher

polarity than PMA, in agreement with the formation of a hydroxylated metabolite. PMA-M1 was not detected in any of the three negative control samples, confirming it to be a metabolite produced by CYP enzymes.

In tier IA samples, two metabolites of PMMA were detected (Table 2). The precursor ion of the first metabolite (PMMA-M1) was *m/z* 166.1234 with the measured DBE value at 4, corresponding to the metabolite resulting from *O*-demethylation of PMMA catalysed by CYPs (Δmass= +4.82 ppm) (Table 2, Fig. 3B). The pattern of the MS/MS spectrum of PMMA-M1 was like that of PMA, suggesting the presence of a hydroxylated group in the *para* position of PMMA-M1 as well. The major fragments of PMMA-M1 included the loss of NH_2CH_3 for *m/z* 135.0798 and the loss of NH_2CH_3 and CH_4 for *m/z* 119.0472 (Table 2, Fig. S2A). The presence of the alkylbenzene moiety was noticed at *m/z* 107.0483, 91.0540, 77.0383 and 65.0380 (see above). The precursor ion of the second metabolite (PMMA-M2) of PMMA was *m/z* 166.1208 (Δmass= +10.8 ppm) and the measured DBE value at 4 (Table 2), which represented the metabolite produced by *N*-demethylation of PMMA by CYP enzymes (Fig. 3B). The structure of PMMA-M2 can be explained by three major product ions and the feature of the alkylbenzene moiety (Table 2, Fig. S2B). A loss of NH_3 for *m/z* 149.0931 remained the common fragment. This ion was further fragmented with a loss of CH_4 and C_2H_4 for the product ions *m/z* 135.0790 and 121.0625, respectively. Both PMMA-M1 and PMMA-M2 eluted several min earlier than PMMA, suggesting that they are more hydrophilic compounds than PMMA, which is consistent with their postulated structures. Furthermore, the retention time of PMMA-M2 was same as that of the PMA standard, which further substantiates its structural identification. Both PMMA-M1 and PMMA-M2 were not detected in any of the three negative control samples, confirming that both PMMA metabolites were produced by CYP enzymes.

Conjugated metabolites of PMA, PMMA and of their CYP-mediated metabolites (i.e. PMA-M1, PMMA-M1 and PMMA-M2) were not detected either in tier IA, nor tier IB

samples. However, in the positive control samples, 4-NP-GLUC and 4-NP-SULF, metabolites of 4-NP produced by UGTs and SULTs, respectively, were detected. This result suggests that the experiment was conducted properly and that both UGTs and SULTs expressed normal catalytic activity. Therefore, the positive control samples substantiated the lack of formation of glucuronidated and sulfated metabolites of PMA-M1, PMMA-M1 and PMMA-M2 under the experimental conditions tested.

PMA-M1 was consistently detected in all tier II samples and not in any of the negative control samples. There was a clear increasing trend of formation of PMA-M1 with incubation times, protein concentrations and substrate concentrations (Figs. 4A-C). This confirmed that PMA-M1 was a metabolite of PMA produced by CYPs. The formation trend of PMA-M1 appeared linked with the reduction of PMA (Figs. 4A-B), providing further evidence of the biotransformation of PMA to PMA-M1.

Similarly, both metabolites of PMMA identified in tier IA were also detected in the tier II samples. The amount of both PMMA-M1 and PMMA-M2 increased with the incubation time, protein concentrations and substrate concentrations (Figs. 4D-F), confirming that PMMA-M1 and PMMA-M2 were the metabolites of PMMA produced by CYP enzymes. In contrast, the parent compound showed an opposite (decreasing) trend. Also, under the different incubation conditions used, PMMA-M1 was formed faster than PMMA-M2 (Figs. 4D-F), suggesting that PMMA-M1 was the primary *in vitro* metabolite of PMMA. Both PMMA-M1 and PMMA-M2 were not detected in any of the three negative control samples, confirming that they were metabolites of PMMA, formed by CYP enzymes. The two data analysis approaches provided consistent results.

2.2. 4-MTA

In tier IA samples, four metabolites (4-MTA-M1, -M2, -M3 and -M4) formed by CYP enzymes were detected (Table 3). None of the four metabolites were detected in any of the three negative control samples. The 4-MTA-M1 precursor ion was *m/z* 198.0946 (Δmass = -

0.50 ppm) and the measured DBE value at 4, representing a hydroxylated metabolite of 4-MTA (Fig. 3C). The structure of 4-MTA-M1 was further elucidated by its MS/MS spectrum (Table 3, Fig. S3A). The loss of NH_3 and $NH_2CH_2CH_3$ gave the product ions *m/z* 181.0674 and 153.0362 respectively. The loss of NH_3 followed by that of CH_3SH from the molecule facilitated the equilibrium moiety between ketone and hydroxyl-ethylene for the fragment ion *m/z* 133.0639. This was likely to further break the OH and C=C bond readily to produce the fragment ion *m/z* 117.0690 and 107.0490, respectively. The characteristic fragment ions for the alkylbenzene moiety were identified at *m/z* 91.0544, 77.0382 and 65.0391. The fragment ions *m/z* 133.0639 and 107.0490 provided consistent evidence that the hydroxyl group was located on the alkyl chain rather than on the benzyl ring of 4-MTA. Also, 4-MTA-M1 eluted about 16 min earlier than 4-MTA, suggesting it was a more polar compound than 4-MTA, which is consistent with its postulated structure. The precursor ion of 4-MTA-M2 was *m/z* 168.0836 (Δmass = -2.97 ppm) with the measured DBE value at 4, matched to a thiol metabolite resulting from *S*-demethylation of 4-MTA (Table 3). The structure of 4-MTA-M2 was postulated by the product ions *m/z* 151.0558 possibly due to the loss of NH_3, 117.0692 likely due to the loss of NH_3 and SH_2, and 91.0536 resulting from the formation of benzylium/tropylium ion (Table 3, Fig. S3B). Also, 4-MTA-M2 eluted about 13 min earlier than 4-MTA (Table 3), suggesting that it is a more polar compound than the substrate.

The 4-MTA-M3 precursor ion was *m/z* 197.0633 (Δmass = +1.01 ppm) with a measured DBE value of 5, and this matched to the metabolite resulting from oxidative deamination of 4-MTA-M1 by CYPs (Table 3, Fig. 3C). The structure of 4-MTA-M3 was postulated by the fragment ion *m/z* 197.0631 (Table 3, Fig. S3C). The acyloin function group, α-hydroxyl ketone, was readily broken to yield the fragment ion *m/z* 137.0411. After that, the fragment ions *m/z* 122.0184 and 121.0095 corresponded to the potential resonance double and triple bonding between the S and C atom [28]. The fragment ions for the alkylbenzene moiety of

358 the 4-MTA-M3 molecule were noticed (Table 3). 4-MTA-M3 eluted about five min later than
359 4-MTA-M2 (Table 3), suggesting it is a less polar compound than 4-MTA-M2.
360 The 4-MTA-M4 precursor ion was *m/z* 199.0787 with the measured DBE value at 4
361 (Table 3, Fig. S3D), corresponding to a di-hydroxylated metabolite of 4-MTA from reduction
362 of 4-MTA-M3 (Fig. 3C). The molecular structure of 4-MTA-M4 was similar to that of 4-
363 MTA-M1 and 4-MTA-M3, as suggested by the common fragment ions present in the MS/MS
364 profiles of these three compounds (Fig. S3). For example, the cleavage of the OH-C=C-OH
365 and the rearrangement of the C-S bond led to the fragment ions *m/z* 122.0156, 121.0097 and
366 107.0491. The loss of $SHCH_3$ from the benzene ring and the dihydroxylated group gave the
367 fragment ion *m/z* 117.0712, which was then further fragmented to form benzylium/tropylium
368 ion *m/z* 91.0547 and the related radical benzene *m/z* 77.0375. 4-MTA-M4 eluted about 6 min
369 earlier than 4-MTA, suggesting it is a more polar compound of 4-MTA due to the addition of
370 two hydroxylated groups.
371 Phase II metabolites of 4-MTA and their CYP-mediated metabolites (i.e. 4-MTA-M1, -
372 M2, -M3 or -M4) were not detected neither in tier IA nor tier IB samples, whereas 4-NP-
373 GLUC and 4-NP-SULF were found in the UGT and SULT positive control samples,
374 respectively. The positive results from the positive control samples supported the lack of
375 formation of glucuronidated and sulfated metabolites of 4-MTA-M1, -M2, -M3 and -M4
376 under the experimental conditions used.
377 In tier II samples, 4-MTA-M1, -M3 and -M4, but not -M2, were detected. These
378 metabolites were not detected in any of the three negative control samples. The formation of
379 4-MTA-M1, -M3 and -M4 increased with incubation time, protein concentration and
380 substrate concentration values used (Fig. 5). In all the analysed samples, 4-MTA-M1 was
381 consistently formed more quickly than 4-MTA-M4, followed by 4-MTA-M3. This result
382 suggested that 4-MTA-M1, -M3 and -M4 were the primary, intermediate and tertiary

metabolite of 4-MTA, respectively, under the range of incubation conditions tested, whereas 4-MTA-M2 was only a minor metabolite of 4-MTA.

2.3. BDB and MBDB

In tier IA samples, no metabolites of BDB produced by CYPs were detected. Only one metabolite of MBDB was detected (MBDB-M1). Its measured precursor ion was *m/z* 194.1174 with the DBE value at 5, which matched to the molecular ion of the *N*-demethylated metabolite of MBDB produced by CYPs (Δmass= +1.03 ppm, Table 4, Fig. 3D). MBDB-M1 was not found in any of the three negative control samples, suggesting that it was a metabolite of MBDB formed by CYP enzymes. The postulated structure of MBDB-M1 was elucidated by its MS/MS profile (Table 4, Fig. S4). The loss of NH_3 from MBDB-M1 ion resulted in the product ion *m/z* 177.0894 which then results in *m/z* 135.0447 due to the loss of the propyl group. With higher collision energy, the dioxolane ring of the MBDB-M1 was broken to form the fragment ions *m/z* 117.0327 and 105.0329. Again, the feature of the alkylbenzene moiety with *m/z* 107.0499, 91.0526 and 77.0391 was detected as the MS/MS fragment ions of MBDB-M1. Also, MBDB-M1 eluted approximately two min earlier than MBDB, suggesting that MBDB-M1 was slightly more polar than MBDB, consistent with its postulated structure. The retention time and the MS/MS fragmentation patterns of MBDB-M1 were as alike as that of BDB. No glucuronidated and sulfated analogues of MBDB and MBDB-M1 were detected in both tier IA and IB samples. Detection of 4-NP-GLUC and 4-NP-SULF in positive control samples substantiated the lack of formation of glucuronidated and sulfated metabolites of MBDB-M1 under the experimental conditions.

MBDB-M1 was detected in all tier II samples, but not found in any of the three negative control samples. No other MBDB metabolites produced by CYPs were detected, which was consistent with the results obtained in tier IA. MBDB-M1 formation increased with incubation times, protein concentrations and substrate concentrations (Fig. 6), providing further evidence that MBDB-M1 was the (only) metabolite of MBDB formed by CYPs. Since

409 no BDB metabolites produced by CYPs were identified in tier I, a tier II experiment was not
410 conducted for BDB.

411 **2.4. 5-APB and 6-APB**

412 No metabolites of 5-APB and 6-APB produced by CYP, UGT and SULT enzymes were
413 detected in any tier I samples. Again, 4-NP-GLUC and 4-NP-SULF were respectively
414 detected in the UGT and SULT positive control samples. Consequently, tier II experiments
415 were not conducted.

416

417 **3. Discussion**

418 This study successfully investigated the formation and characterisation of *in vitro*
419 metabolites of seven phenethylamine-based designer drugs using HLM and LC-QTOF-MS.
420 In tier IA, structures of the possible metabolites were predicted through interpreting the
421 potential enzymatically-catalysed reactions between the parent drug and the family of
422 enzymes selected. Since reference standards for the CYP-produced metabolites detected in
423 tier IA may not be always available from commercial laboratories, the current study included
424 tier IB experiments, in which these primary metabolites were enzymatically generated and
425 then incubated with the enzyme mixture containing the Phase II enzyme families (i.e. UGTs
426 and SULTs). Furthermore, this study presented tier II experiments as an extended approach to
427 confirm the metabolites identified in tier I, by understanding the formation profiles of the
428 metabolites according to three different experimental conditions. With such multiple testing
429 conditions, the work overall provides a comprehensive assessment of the *in vitro* experiments
430 for higher reproducibility and consistency of *in vitro* metabolism data. It should be noted that
431 careful attention has been paid to the preparation of the reaction mixture in this study:
432 particularly, (a) the organic solvent content was kept at maximum 1% of the reaction mixture
433 to minimise its dose-dependent impact on the enzyme catalytic activity [29, 30]; (b) the
434 NADPH was replenished every hour to counterbalance its deterioration over time and to thus

435 maintain its concentration close to saturation [31]; (c) the final protein concentration in each
436 sample was kept below 1 mg/mL to avoid large extents of non-specific protein binding of the
437 substrate [32, 33]; (d) a three-hour long incubation was conducted in tier IB to generate
438 enough Phase I metabolites for further Phase II reactions (Fig. 2); (e) positive and negative
439 control samples were prepared as quality controls of the experiments for justifying the
440 obtained results; (f) theophylline (which ionises in both positive and negative modes) was
441 chosen as the internal standard to compensate variations during sample preparation and
442 analytical measurements.

443 This study showed that the *in vitro* metabolism of PMA and PMMA was relatively slow,
444 with only one metabolite (*para*-hydroxyamphetamine) formed from PMA and two
445 metabolites (primary: *para*-hydroxymethamphetamine; secondary: PMA) from PMMA. As
446 they share a phenethylamine moiety, the proposed pathway of PMA and PMMA metabolism
447 in the present study was in agreement with that of other illicit phenethylamine drugs. For
448 example, both amphetamine and methamphetamine are not extensively metabolised in
449 humans (about 30% and 40% of the parent compound is measured in human urine,
450 respectively) [34]. The primary metabolite of PMA and PMMA (PMA-M1 and PMMA-M1,
451 respectively) was mainly produced by CYP-mediated *O*-demethylation. However, this
452 reaction occurred approximately 10 to 20 times faster for PMMA than for PMA, which was
453 observed consistently with increasing experimental times, enzyme concentrations, and
454 substrate concentrations (see red symbols in Fig. 4). Since the structural difference between
455 PMA and PMMA is only the methylation of the amino group (for PMMA), the obtained data
456 suggest that the presence of the methylated amino group substantially favoured an *O*-
457 dealkylation metabolism pathway to produce *para*-hydroxyl metabolites. Similar results were
458 also obtained in previous studies when comparing amphetamine and methamphetamine *in*
459 *vivo* metabolism in humans. While the *para*-hydroxyl metabolite is common for
460 amphetamine and methamphetamine, its formation is more pronounced for methamphetamine

than amphetamine (15% *vs.* 3%, respectively) [34-36]. Moreover, the *in vitro* metabolism of PMMA investigated in this study showed that the *N*-dealkylation reaction was about five to seven times less favourable than the *O*-dealkylation (see red and purple symbols in Figs. 4D-F). This is consistent with *N*-demethylation of methamphetamine to amphetamine (about 4-7% of a methamphetamine dose excreted in urine), occurring only to a very small extent [34].

The metabolites of PMA and PMMA detected in this study are generally consistent with those reported in the literature. PMA-M1 was the major *in vitro* metabolite produced by CYP2D6 [18] and the major *in vivo* metabolite in urine samples of three healthy volunteers who consumed PMA [37, 38] (Table S1). Similarly, CYP2D6 has been found to mediate the *in vitro* formation of PMMA-M1 in humans [19, 20, 38]. To our knowledge, *in vivo* metabolism studies of PMMA are not available for humans, only for rats [39]. In urine samples collected from rats administered with PMMA, PMMA-M1 and PMMA-M2 were the major and the minor metabolites detected, respectively (Table S1). This result is in agreement with the *in vitro* data of this study, implying a common metabolism pathway of PMMA in rats and humans.

Glucuronidated PMA-M1 was occasionally detected in the urine samples of the three volunteers [37] (Table S1). For glucuronidated and/or sulfated metabolites of PMMA, minor amounts were found in the rat urine [39] (Table S1). Similarly, urinary excretion of conjugated metabolites for amphetamine and methamphetamine was observed only to a small extent in humans [34-36]. Taken together, these findings consistently reveal that *in vivo* glucuronidation and sulfation is not a major part of the metabolic pathway of PMA and PMMA in humans and rats. This finding is coherent with the lack of detection of PMA and PMMA Phase II metabolites in the *in vitro* metabolism experiments of this study.

This study revealed that 4-MTA was largely metabolised into four metabolites (Table 3) and a clear trend of their formation was observed (Fig. 5). The results also suggest that the mechanism of the CYP-mediated metabolism of 4-MTA is different from that of PMA and

PMMA. The primary metabolite (4-MTA-M1) of 4-MTA is a mono-hydroxylated metabolite (4-methylthiocathine), most likely formed by oxidation of an unsubstituted C atom, catalysed by CYPs. In spite of sharing similar chemical structures among 4-MTA, PMA and PMMA, this mono-hydroxylated metabolite was not detected for PMA or PMMA. This implies that the presence of the S atom in 4-MTA at the *para* position of the phenethylamine-based chemical structure favours such oxidative metabolism rather than the O atom in PMA and PMMA. To a dealkylation reaction for such *para*-substituted phenethylamine compounds, the obtained data reveal that with CYP enzymes, *S*-dealkylation is much less favourable than *O*-dealkylation reaction. This was observed from the result that the *S*-demethylated metabolite (4-MTA-M2) of 4-MTA was only detected after the three-hour long incubations (the first set of tier IB), whereas the *O*-demethylated metabolite of PMA and PMMA were readily generated after 10 min (Fig. 4). The tier II data of 4-MTA provided an indication that 4-MTA-M1 is transformed by CYPs to the corresponding ketone (4-MTA-M3, secondary or intermediate metabolite) through an oxidative deamination (Fig. 3C). It is then reduced to a di-hydroxylated metabolite (4-MTA-M4, tertiary metabolite, Fig. 3C), showing a similar metabolism pattern to 4-MTA-M1 (see red and green symbols in Fig. 5).

Even less is known about 4-MTA metabolism than that for PMA and PMMA. 4-Methylthiobenzoic acid was reported as the major metabolite when incubating 4-MTA with human hepatocytes obtained from three volunteers [40], but this metabolite was not detected in this study. The discrepancy might be due to the lack of the enzymes for producing 4-methylthiobenzoic acid in HLM. In contrast, unchanged 4-MTA was found as the major compound in five human urine samples (Table S1) with a few minor metabolites identified which were formed via oxidative deamination followed by reduction to corresponding alcohol and degradation of the side change to 4-methylthiobenzoic acid [41]. Metabolites of ring- and β-hydroxylation (4-methylthiocathine, i.e. 4-MTA-M1 in this study) were detected in the urine samples too [41]. Similar metabolites were also observed in mice urine samples

513 [42] (Table S1), including unchanged 4-MTA, 4-methylthiobenzoic acid, 4-methylthiocathine
514 and hydroxyl-4-MTA on the aromatic ring and the methylthio-side chain; however,
515 conjugation of these metabolites was hardly observed. While the identified *in vivo* and *in*
516 *vitro* metabolites of 4-MTA partly agree with this and previous studies [40-42], the current
517 study provides additional information on *in vitro* metabolism of 4-MTA using CYPs.

518 The obtained *in vitro* metabolism data on MBDB, BDB, 5-APB and 6-APB by HLM and
519 HLCYT consistently indicate that these drugs are hardly metabolised. The only metabolite of
520 MBDB was detected via an *N*-dealkylation reaction (MBDM-M1; Table 4, Fig. 3D). The
521 difference in the chemical structure between MBDB and BDB is only the methylation of the
522 amino group (for MBDB). The data again showed that dealkylation metabolism is more
523 favourable at the amino than at the methyl group, consistent with what has been noticed for
524 PMMA metabolism (Figs. 4D-F). The consistent formation pattern between MBDB-M1 and
525 PMMA-M2 (see red symbols in Fig. 6 and purple symbols in Figs. 4D-F) implies that the *N*-
526 dealkylation metabolism pathway for such phenethylamine-based designer drugs in general
527 proceeds at a very slow pace. Furthermore, the lack of detection of any metabolites for BDB,
528 5-APB and 6-APB reinforces the role of methylation of the amino group in favouring the *in*
529 *vitro* metabolism for this group of drugs as this moiety is the major structural difference
530 among them.

531 The results of this study are partially in line with other metabolism studies for these four
532 drugs. For example, MBDB-M1 (i.e. BDB) was the major metabolite of MBDB in which
533 CYP2B6 is supposed to mediate this *N*-demethylation metabolic pathway [21, 22]. Although
534 the catechol metabolite of MBDB and BDB through mediation of CYP2D6 for demethylation
535 [22, 23] was detected in the human and rat urine samples [21] (Table S1), this metabolite has
536 been found to be unstable in the *in vitro* assays [21, 43]. The lack of detection of the catechol
537 metabolite for MBDB and BDB in this study could be explained by this previous finding
538 and/or because its amounts would have been too low in the *in vitro* samples for the QTOF-

539 MS detection limit. The latter reason could also explain the lack of detection of *N*-
540 demethylated metabolite for BDB. The data obtained are consistent with the previous study
541 showing that glucuronidated and sulfated conjugated metabolites of MBDB and BDB were
542 not detected in the *in vitro* experiments using particular isoenzymes of human and rat [21].
543 These results overall suggest that conjugation of MBDB and BDB appears not to be a major
544 part of their metabolic pathway in humans. Human *in vitro* metabolism studies for 5-APB
545 and 6-APB are very limited in the literature and thus *in vitro* metabolites of these drugs are
546 not yet well-known so far [44]. While this study has found that the metabolism process of 5-
547 and 6-APB was very slow, one study [45] has very recently shown similar results, in that only
548 limited amounts of *in vitro* metabolites of 5-APB, including hydroxyl-5-APB, hydroxy-
549 dihydro-5-APB and 3-carboxymethyl-4-hydroxy amphetamine, were yielded and its
550 formation rate was very low. *In vivo* metabolites of 5-APB were recently reported in rat urine
551 [45] but are not yet known in human urine (Table S1). Similar to the present *in vitro* study, 5-
552 APB and 6-APB were not degraded by activated sludge (own unpublished data). These
553 findings suggest that these two drugs are rather resistant to enzymatic and bacterial
554 digestions.

555 *In vitro* metabolism data of the selected designer drugs are important for drug-related
556 disciplines, such as forensic toxicology, since they provide key compounds useful to better
557 identify these drugs in humans and crime scenes. Also, the results of the current study reveal
558 potential human biomarkers of the targeted designer drugs to be measured in urine from
559 individuals, pooled urine samples or even wastewater samples for assessing the use of these
560 designer drugs in the emerging research field of wastewater-based drug epidemiology [46].
561 Since the data indicated that the *in vitro* metabolism of the targeted designer drugs proceeds
562 at slow rate, the parent drug itself appears to be the key biomarker in most cases. However,
563 for PMA and PMMA, the respective *para*-hydroxylated metabolite can be considered as its
564 second target biomarker. Also, it should be noted that since PMMA-M2 (i.e. PMA) was only

565 the secondary metabolite of PMMA, high levels of PMA detection in human fluids and
566 wastewater samples may reflect the use PMA rather than that of PMMA. From the current *in*
567 *vitro* experiments of 4-MTA, 4-methylthiocathine (4-MTA-M1) can be regarded as its key
568 biomarker, with the di-hydroxylated metabolite (4-MTA-M4) as its second major biomarker.
569 In future studies, *in vitro* experiments can provide further support to identify suitable
570 biomarkers in the matrix of interest. For this purpose, the database of retention times, MS and
571 MS/MS spectra of each metabolite detected *in vitro* represents a valuable tool to confirm the
572 identity of the biomarkers detected in (*in vivo*) samples, particularly when no authentic
573 reference standards for any of these metabolites/biomarkers are commercially available. It
574 should be noted that further research is needed to examine whether those potential
575 biomarkers are stable in wastewater before they can be used for reliable monitoring of drug
576 use in wastewater-based drug epidemiology.
577
578 **4. Conclusions**
579 Overall, the work of this study has, for the first time, (a) screened for human *in vitro*
580 metabolites of the selected phenethylamine-based designer drugs using an untargeted analysis
581 of LC-QTOF-MS, and also (b) described a stepwise *in vitro* experimental design to enhance
582 the reliability of assessing *in vitro* drug metabolism. The metabolism of the targeted drugs
583 was mainly catalysed by CYP enzymes and progressed at relatively slow rate with only
584 limited number of metabolites formed. The *in vitro* metabolism pathway of the selected drugs
585 preferentially proceeded via *O*-dealkylation followed by *N*-dealkylation, and to a much
586 smaller extent, oxidation of unsubstituted carbon atoms and oxidative deamination. The *in*
587 *vitro* metabolism results broadly agreed with the findings of other available metabolism
588 studies for phenethylamine-based drugs. The current work has established a list of specific *in*
589 *vitro* human metabolites for the targeted drugs which are beneficial to all kinds of drug-
590 related disciplines, such as clinical and forensic toxicology and the emerging research field of

591 wastewater-based drug epidemiology, for better detection and monitoring of the use of these
592 drugs in humans and communities.
593
594 **Acknowledgements**
595 The National Research Centre for Environmental Toxicology (Entox) is a joint venture
596 of The University of Queensland (UQ) and Queensland Health Forensic Scientific Services
597 (QHFSS). The authors sincerely thank Nele Van den Eede (University of Antwerp (UA)) and
598 Walid Maho (UA) for advising on the operation of the LC-QTOF-MS instrument. We also
599 would like to acknowledge Xiaobo Zheng (UA) for assistance with the sample preparation
600 and Maria Jose Gomez Ramos (Entox, UQ) and Nele Van den Eede for the discussion on
601 fragmentation in mass spectrometry. We sincerely thank Dr. Raimondo Bruno (University of
602 Tasmania, Australia) for his valuable input on discussions and language revisions. Foon Yin
603 Lai is funded through UQ Collaboration and Industry Engagement Fund (UQCIEF #608290)
604 and Collaborative Research Seeding Grants of the Faculty of Health and Behavioural
605 Sciences (UQHABS #608670). Alexander L.N. van Nuijs acknowledges FWO Flanders for
606 his scholarship. The research leading to these results has received funding from the European
607 Union Seventh Framework Programme (FP7/2007-2013) under grant agreement #295138
608 (INTERFLAME project), #316665 (A-TEAM project) and #317205 (SEWPROF project).
609
610 **Conflict of interest**
611 None

References

[1] UNODC. World Drug Report 2013. United Nations Office of Drugs and Crime (UNODC), United Nations publication, Sales No E13XI6, 2013.

[2] UNODC. The Challenge of New Psychoactive Substances. United Nations Office of Drugs and Crime (UNODC), A Report from the Global SMART Programme, March 2013.

[3] L.A. King, A.T. Kicman. A brief history of 'new psychoactive substances'. Drug Test Anal 3 (2011) 401-3.

[4] I. Sample. 'Superman' pill deaths spark calls for dangerous-drugs alert system. The Guardian 17 January 2015. Available at: http://wwwtheguardiancom/society/2015/jan/16/superman-pill-deaths-dangerous-drugs-alert-system [accessed 26 February 2015]

[5] D. Nutt. The Superman pill deaths are the result of our illogical drugs policy The Guardian 5 January 2015. Available at: http://wwwtheguardiancom/commentisfree/2015/jan/05/superman-pill-ecstasy-pma-deaths-drugs-policy [accessed 26 February 2015]

[6] Australian Broadcasting Corporation (ABC). Potentially lethal 'Superman' drug could be on sale in Australia, police warn. ABC 25 February 2015 Available at: http://wwwtheguardiancom/commentisfree/2015/jan/05/superman-pill-ecstasy-pma-deaths-drugs-policy [accessed 26 February 2015]

[7] E. Zuccato, C. Chiabrando, S. Castiglioni, *et al.* Estimating community drug abuse by wastewater analysis. Environ Health Perspect 116 (2008) 1027-32.

[8] K.V. Thomas, L. Bijlsma, S. Castiglioni, *et al.* Comparing illicit drug use in 19 European cities through sewage analysis. Sci Total Environ 432 (2012) 432-9.

[9] C. Chen, C. Kostakis, R.J. Irvine, *et al.* Increases in use of novel synthetic stimulant are not directly linked to decreased use of 3,4-methylenedioxy-*N*-methylamphetamine (MDMA). Forensic Sci Int 231 (2013) 278-83.

[10] A.L.N. van Nuijs, A. Gheorghe, P.G. Jorens, *et al.* Optimization, validation, and the application of liquid chromatography-tandem mass spectrometry for the analysis of new drugs of abuse in wastewater. Drug Test Anal 6 (2014) 861-7.

[11] M.J. Reid, L. Derry, K.V. Thomas. Analysis of new classes of recreational drugs in sewage: Synthetic cannabinoids and amphetamine-like substances. Drug Test Anal 6 (2014) 72-9.

[12] A. Kankaanpää, K. Ariniemi, M. Heinonen, *et al.* Use of illicit stimulant drugs in Finland: a wastewater study in ten major cities. Sci Total Environ 487 (2014) 696-702.

[13] J. Kinyua, A. Covaci, W. Maho, *et al.* Sewage-based epidemiology in monitoring the use of new psychoactive substances: Validation and application of an analytical method using LC-MS/MS. Drug Test Anal (2015). DOI: 10.1002/dta.1777.

[14] Peters FT, Meyer MR. *In vitro* approaches to studying the metabolism of new psychoactive compounds. Drug Test Anal 3 (2011) 483-95.

[15] Z.Y. Liu. An introduction to hybrid ion trap/time-of-flight mass spectrometry coupled with liquid chromatography applied to drug metabolism studies. J Mass Spectrom 47 (2012) 1627-42.

[16] D. Spaggiari, L. Geiser, S. Rudaz. Coupling ultra-high-pressure liquid chromatography with mass spectrometry for in-vitro drug-metabolism studies. Trac-Trend Anal Chem 63 (2014) 129-39.

[17] European Monitoring Center for Drugs and Drug Addiction (EMCDDA). Action on new drugs. Risk assessments. EMCDDA, Lisbon. Available at: http://www.emcdda.europa.eu/html.cfm/index16776EN.html [accessed 26 February 2015].

[18] M.V. Bach, R.T. Coutts, G.B. Baker. Involvement of CYP2D6 in the *in vitro* metabolism of amphetamine, two *N*-alkylamphetamines and their 4-methoxylated derivatives. Xenobiotica 29 (1999) 719-32.

[19] R.F. Staack, D.S. Theobald, L.D. Paul, *et al.* Identication of human cytochrome P450 2D6 as major enzyme involved in the *O*-demethylation of the designer drug *p*-methoxymethamphetamine. Drug Metab Dispos 32 (2004) 379-81.

[20] R.T. Coutts, O.O. Bolaji, P. Su, *et al.* Metabolism of methoxyphenamine *in vitro* by a CYP2D6 microsomal preparation. Drug Metab Dispos 22 (1994) 756-60.

[21] H.H. Maurer, J. Bickeboeller-Friedrich, T. Kraemer, *et al.* Toxicokinetics and analytical toxicology of amphetamine-derived designer drugs ('Ecstasy'). Toxicol Lett 112-113 (2000) 133-42.

[22] M.R. Meyer, F.T. Peters, H.H. Maurer. Stereoselective differences in the cytochrome P450-dependent dealkylation and demethylenation of *N*-methyl-benzodioxolyl-butanamine (MBDB, Eden) enantiomers. Biochem Pharmacol 77 (2009) 1725-34.

[23] M.R. Meyer, F.T. Peters, H.H. Maurer. Investigations on the human hepatic cytochrome P450 isozymes involved in the metabolism of 3,4-methylenedioxy-amphetamine (MDA) and benzodioxolyl-butanamine (BDB) enantiomers. Toxicol Lett 190 (2009) 54-60.

[24] N. van den Eede, W. Maho, C. Erratico, *et al.* First insights in the metabolism of phosphate flame retardants and plasticizers using human liver fractions. Toxicol Lett 223 (2013) 9-15.

[25] A. Ballesteros-Gómez, C. Erratico, N. van den Eede, *et al. In vitro* metabolism of 2-ethylhexyldiphenyl phosphate (EHDPHP) by human liver microsomes. Toxicol Lett 232 (2015) 203-12.

[26] E. Tyrkkö, A. Pelander, R. Ketola, *et al. In silico* and *in vitro* metabolism studies support identification of designer drugs in human urine by liquid chromatography/quadrupole-time-of-flight mass spectrometry. Anal Bioanal Chem 405 (2013) 6697-709.
[27] B. Chiavarino, M.E. Crestoni, O. Dopfer, *et al.* Benzylium versus tropylium ion dichotomy: vibrational spectroscopy of gaseous $C_8H_9^+$ ions. Angew Chem Int Edit 51 (2012) 4947-9.
[28] P.R. Schreiner, H.P. Reisenauer, J. Romanski, *et al.* A formal carbon-sulfur triple bond: H-C≡S-O-H. Angew Chem Int Edit 48 (2009) 8133-6.
[29] N. Chauret, A. Gauthier, D.A. Nicoll-Griffith. Effect of common organic solvents on *in vitro* cytochrome P450-mediated metabolic activities in human liver microsomes. Drug Metab Dispos 26 (1998) 1-4.
[30] D. Li, Y. Han, X. Meng, *et al.* Effect of regular organic solvents on cytochrome P450-mediated metabolic activities in rat liver microsomes. Drug Metab Dispos 38 (2010) 1922-5.
[31] J.T. Wu, L.H. Wu, J.A. Knight. Stability of NADPH: effect of various factors on the kinetics of degradation. Clin Chem 32 (1986) 314-9.
[32] R.S. Obach. Nonspecific binding to microsomes: impact on scale-up of *in vitro* intrinsic clearance to hepatic clearance as assessed through examination of warfarin, imipramine, and propranolol. Drug Metab Dispos 25 (1997) 1359-69.
[33] K. Venkatakrishnan, L.L. von Moltke, R.S. Obach, *et al.* Microsomal binding of amitriptyline: effect on estimation of enzyme kinetic parameters *in vitro*. J Pharmacol Exp Ther 293 (2000) 343-50.
[34] R. Baselt. Disposition of Toxic Drugs and Chemicals in Man. Foster City: CA: Biomedical Publications; (2008).
[35] L.G. Dring, R.L. Smith, R.T. Williams. The metabolic fate of amphetamine in man and other species. Biochem J 116 (1970) 425-35.
[36] I. Kim, J.M. Oyler, E.T. Moolchan, *et al.* Urinary pharmacokinetics of methamphetamine and its metabolite, amphetamine following controlled oral administration to humans. Ther Drug Monit 26 (2004) 664-72.
[37] I. Kitchen, J. Tremblay, J. André, *et al.* Interindividual and interspecies variation in the metabolism of the hallucinogen 4-methoxyamphetamine. Xenobiotica 9 (1979) 397-404.
[38] R.F. Staack, H.H. Maurer. Metabolism of designer drugs of abuse. Curr Drug Metab 6 (2005) 259-74.
[39] R.F. Staack, J. Fehn, H.H. Maurer. New designer drug *p*-methoxymethamphetamine: studies on its metabolism and toxicological detection in urine using gas chromatography-mass spectrometry. J Chromatogr B 789 (2003) 27-41.
[40] H. Carmo, J. Hengstler, D. de Boer, *et al.* Comparative metabolism of the designer drug 4-methylthioamphetamine by hepatocytes from man, monkey, dog, rabbit, rat and mouse. N-S Arch Pharmacol 369 (2004) 198-205.
[41] A.H. Ewald, F.T. Peters, M. Weise, *et al.* Studies on the metabolism and toxicological detection of the designer drug 4-methylthioamphetamine (4-MTA) in human urine using gas chromatography-mass spectrometry. J Chromatogr B 824 (2005) 123-31.
[42] H. Carmo, D. de Boer, F. Remião, *et al.* Identification of 4-methylthioamphetamine and some of its metabolites in mouse urine by GC-MS after acute administration. J Anal Toxicol 26 (2002) 228-32.
[43] H.H. Maurer. On the metabolism and the toxicological analysis of methylenedioxyphenylalkylamine designer drugs by gas chromatography-mass spectrometry. Ther Drug Monit 18 (1996) 465-70.
[44] Kronstrand R. Emerging Designer Drug Monograph. Society of Forensic Toxicologists, Inc Designer Drug Committee Monographs vers 11, 2013.
[45] Welter J., Kavanagh P., Meyer M., *et al.* Benzofuran analogues of amphetamine and methamphetamine: studies on the metabolism and toxicological analysis of 5-APB and 5-MAPB in urine and plasma using GC-MS and LC-(HR)-MS^n techniques. Anal Bioanal Chem (2014) 1-18.
[46] A.L.N. van Nuijs, S. Castiglioni, I. Tarcomnicu, *et al.* Illicit drug consumption estimations derived from wastewater analysis: A critical review. Sci Total Environ 409 (2011) 3564-77.

721 **Tables**

722

723 **Table 1:** Postulated structure for PMA metabolite generated from incubation with HLM in tier I.

ID Met	Precursor ion (MS-TOF)				Product ions* (MS/MS-TOF)			
	Measured m/z $[M+H]^+$	Expected m/z (ppm diff.)	Measured DBE	RT (min)	Measured m/z	Expected m/z (ppm diff.)	Potential fragment structure [molecular formula]	Proposed structure
M1	152.1063 $[C_9H_{13}NO+H]^+$	152.1070 (+4.60)	4	5.17	135.0799	135.0810 (-8.14)	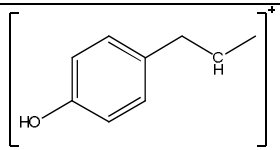 $[C_9H_{11}O]^+$	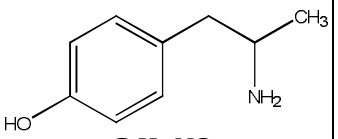 $C_9H_{13}NO$
					107.0495	107.0497 (-1.87)	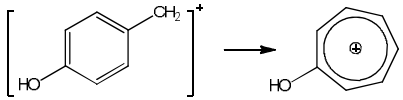 $[C_7H_7O]^+$	
					91.0552	91.0548 (+4.39)	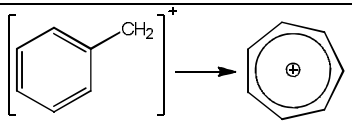 $[C_7H_7]^+$	
					77.0390	77.0386 (+5.19)	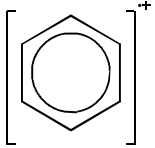 $[C_6H_5]^{\bullet+}$	
					65.0364	65.0386 (-33.8)	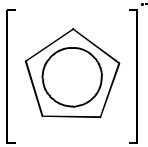 $[C_5H_5]^{\bullet+}$	

ID Met: Identified metabolite; m/z: mass to charge ratio; DBE: double bond equivalents.
*See Fig. S1 for the MS/MS-TOF spectrum.

724

725 **Table 2:** Postulated structures for PMMA metabolites generated from incubation with HLM in tier I.

ID Met	Precursor ion (MS-TOF)				Product ions* (MS/MS-TOF)			
	Measured m/z $[M+H]^+$	**Expected m/z (ppm diff.)**	**Measured DBE**	**RT (min)**	**Measured m/z**	**Expected m/z (ppm diff.)**	**Potential fragment structure [molecular formula]**	**Proposed structure**
M1	166.1234 $[C_{10}H_{15}NO+H]^+$	166.1226 (+4.82)	4	5.40	135.0798	135.0810 (-8.88)	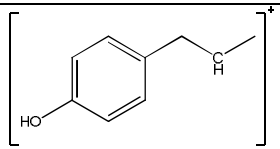 $[C_9H_{11}O]^+$	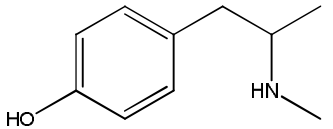 $C_{10}H_{15}NO$
					119.0472	119.0497 (-21.0)	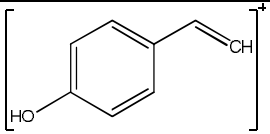 $[C_8H_7O]^+$	
					107.0483	107.0497 (-13.1)	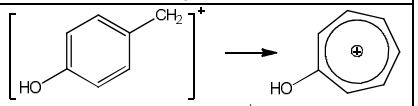 $[C_7H_7O]^+$	
					91.0540	91.0548 (-8.79)	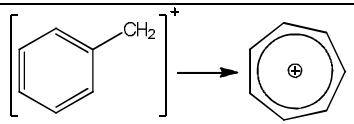 $[C_7H_7]^+$	
					77.0383	77.0386 (+3.89)	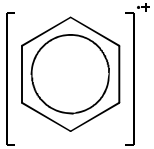 $[C_6H_5]^{\bullet+}$	
					65.0380	65.0386 (-9.23)	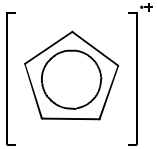 $[C_5H_5]^{\bullet+}$	

M2	166.1208 $[C_{10}H_{15}NO+H]^+$	166.1226 (+10.8)	4	15.6	149.0931	149.0966 (-23.5)	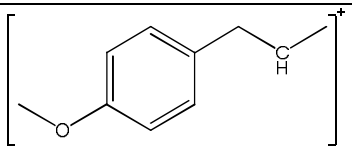 $[C_{10}H_{13}O]^+$	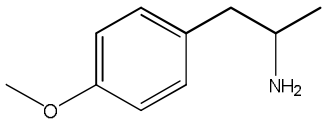 $C_{10}H_{15}NO$
					135.0790	135.0810 (-14.8)	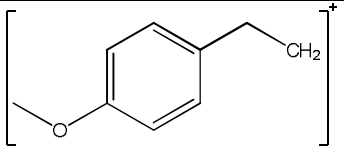 $[C_9H_{11}O]^+$	
					121.0625	121.0653 (-23.1)	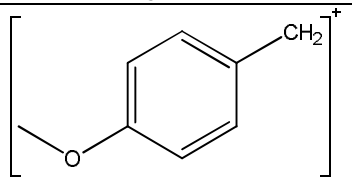 $[C_8H_9O]^+$	
					91.0523	91.0548 (-27.5)	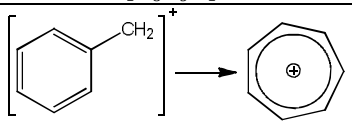 $[C_7H_7]^+$	
					77.0371	77.0386 (-19.5)	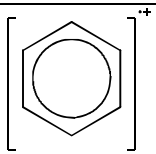 $[C_6H_5]^{\bullet+}$	
					65.0364	65.0386 (-33.8)	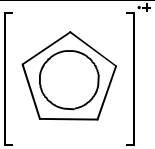 $[C_5H_5]^{\bullet+}$	

ID Met: Identified metabolite; m/z: mass to charge ratio; DBE: double bond equivalents.
*See Figs. S2A and S2B for the MS/MS-TOF spectrum.

726

727 **Table 3:** Postulated structures for 4-MTA metabolites generated from incubation with HLM in tier I.

ID Met	Precursor ion (MS-TOF)				Product ions* (MS/MS-TOF)			
	Measured m/z $[M+H]^+$	**Expected m/z (ppm diff.)**	**Measured DBE**	**RT (min)**	**Measured m/z**	**Expected m/z (ppm diff.)**	**Potential fragment structure [molecular formula]**	**Proposed structure**
M1	198.0946 $[C_{10}H_{15}NOS+H]^+$	198.0947 (-0.50)	4	6.20	181.0674	181.0687 (-7.18)	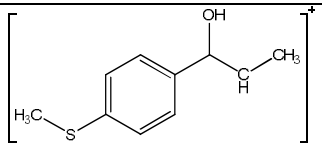 $[C_{10}H_{13}OS]^+$	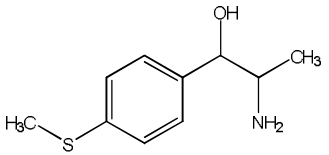 $C_{10}H_{15}NOS$
					153.0362	153.0374 (-7.84)	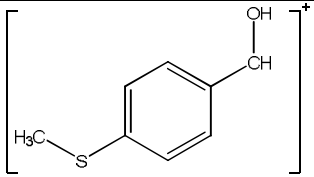 $[C_8H_9OS]^+$	
					133.0639	133.0648 (-6.76)	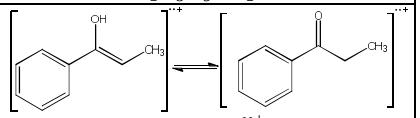 $[C_9H_9O]^{\bullet+}$	
					117.0690	117.0699 (-7.69)	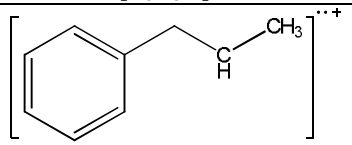 $[C_9H_9]^{\bullet+}$	
					107.0490	107.0491 (-0.93)	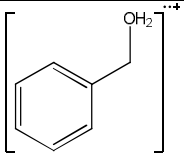 $[C_7H_7O]^{\bullet+}$	
					91.0544	91.0548 (-4.39)	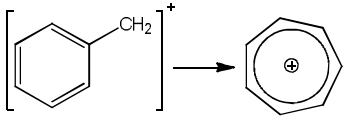	

							$[C_7H_7]^+$	
					77.0382	77.0386 (-5.19)	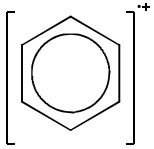 $[C_6H_5]^{\bullet+}$	
					65.0391	65.0386 (+7.69)	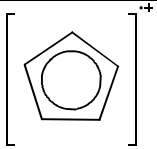 $[C_5H_5]^{\bullet+}$	
M2	168.0836 $[C_9H_{13}NS+H]^+$	168.0841 (-2.97)	4	8.94	151.0558	151.0581 (-15.2)	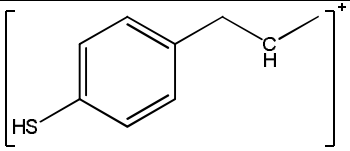 $[C_9H_{11}S]^+$	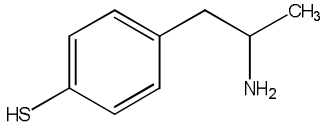 $C_9H_{13}NS$
					117.0692	117.0699 (-5.98)	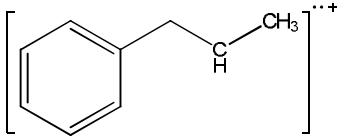 $[C_9H_9]^{\bullet\bullet+}$	
					91.0536	91.0548 (-13.2)	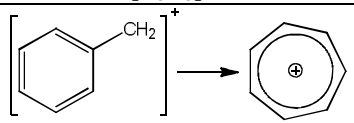 $[C_7H_7]^+$	
M3	197.0633 $[C_{10}H_{12}O_2S+H]^+$	197.0631 (+1.01)	5	14.1	137.0411	137.0425 (-10.2)	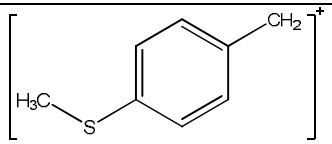 $[C_8H_9S]^+$	

					122.0184	122.0185 (-0.82)	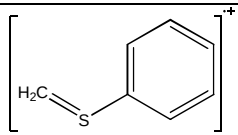 $[C_7H_6S]^{\bullet+}$	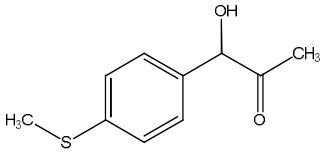 $C_{10}H_{12}O_2S$
					121.0095	121.0106 (-9.09)	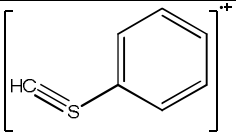 $[C_7H_5S]^{\bullet+}$	
					89.0389	89.0386 (+3.37)	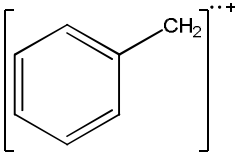 $[C_7H_5]^{\bullet\bullet+}$	
					77.0385	77.0386 (-1.30)	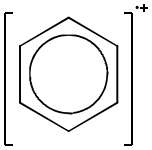 $[C_6H_5]^{\bullet+}$	
					65.0388	65.0386 (+3.08)	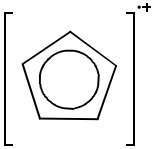 $[C_5H_5]^{\bullet+}$	
M4	199.0787 $[C_{10}H_{14}O_2S+H]^+$	199.0787 (0.00)	4	15.4	122.0156	122.0185 (-23.8)	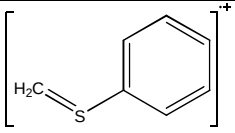 $[C_7H_6S]^{\bullet+}$	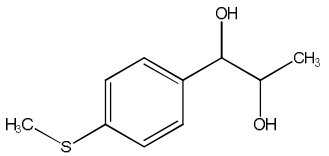 $C_{10}H_{14}O_2S$
					121.0097	121.0106 (-7.44)	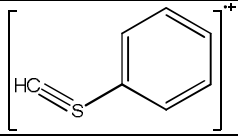	

							$[C_7H_5S]^{\bullet+}$	
					117.0712	117.0699 (+11.1)	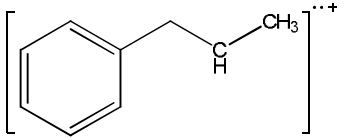 $[C_9H_9]^{\bullet\bullet+}$	
					107.0491	107.0491 (0.00)	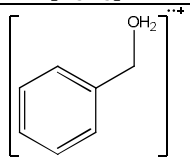 $[C_7H_7O]^{\bullet\bullet+}$	
					91.0547	91.0548 (-1.10)	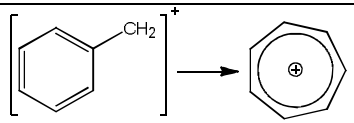 $[C_7H_7]^{+}$	
					77.0375	77.0386 (-14.3)	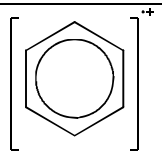 $[C_6H_5]^{\bullet+}$	

ID Met: Identified metabolite; m/z: mass to charge ratio; DBE: double bond equivalents.
*See Figs. S3A to 3D for the MS/MS-TOF spectrum.

730 **Table 4:** Postulated structure for MBDB metabolite generated from incubation with HLM in tier I.

ID Met	Precursor ion (MS-TOF)				Product ions* (MS/MS-TOF)			
	Measured m/z $[M+H]^+$	**Expected m/z (ppm diff.)**	**Measured DBE**	**RT (min)**	**Measured m/z**	**Expected m/z (ppm diff.)**	**Potential fragment structure [molecular formula]**	**Proposed structure**
M1	194.1174 $[C_{11}H_{15}NO_2 +H]^+$	194.1176 (+1.03)	5	18.7	177.0894	177.0916 (-12.4)	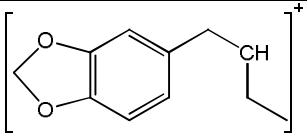 $[C_{11}H_{13}O_2]^+$	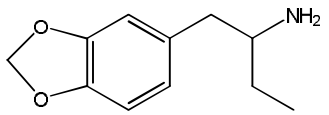 $C_{11}H_{15}NO_2$
					135.0447	135.0446 (+0.74)	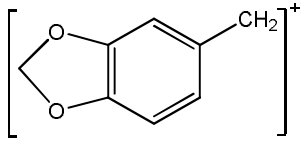 $[C_8H_7O_2]^+$	
					117.0327	117.0335 (-6.84)	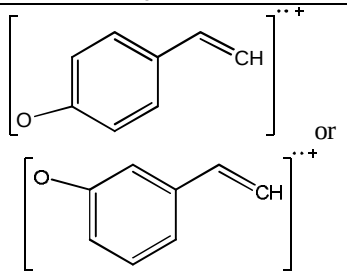 $[C_8H_5O]^{\bullet+}$	
					107.0499	107.0497 (+1.87)	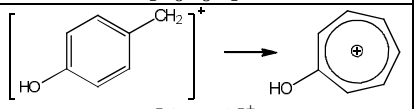 $[C_7H_7O]^+$	
					105.0329	105.0335 (-5.71)	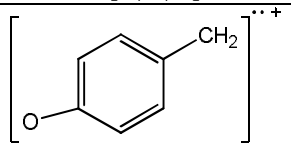	

							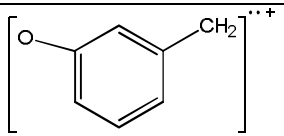 $[C_7H_5O]^{\bullet\bullet+}$	
					91.0526	91.0548 (-24.2)	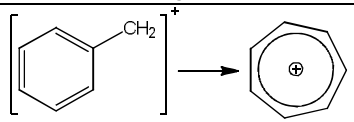 $[C_7H_7]^+$	
					77.0391	77.0386 (+6.49)	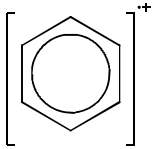 $[C_6H_5]^{\bullet+}$	
ID Met: Identified metabolite; m/z: mass to charge ratio; DBE: double bond equivalents. *See Fig. S4 for the MS/MS-TOF spectrum.								

731
732

Figures

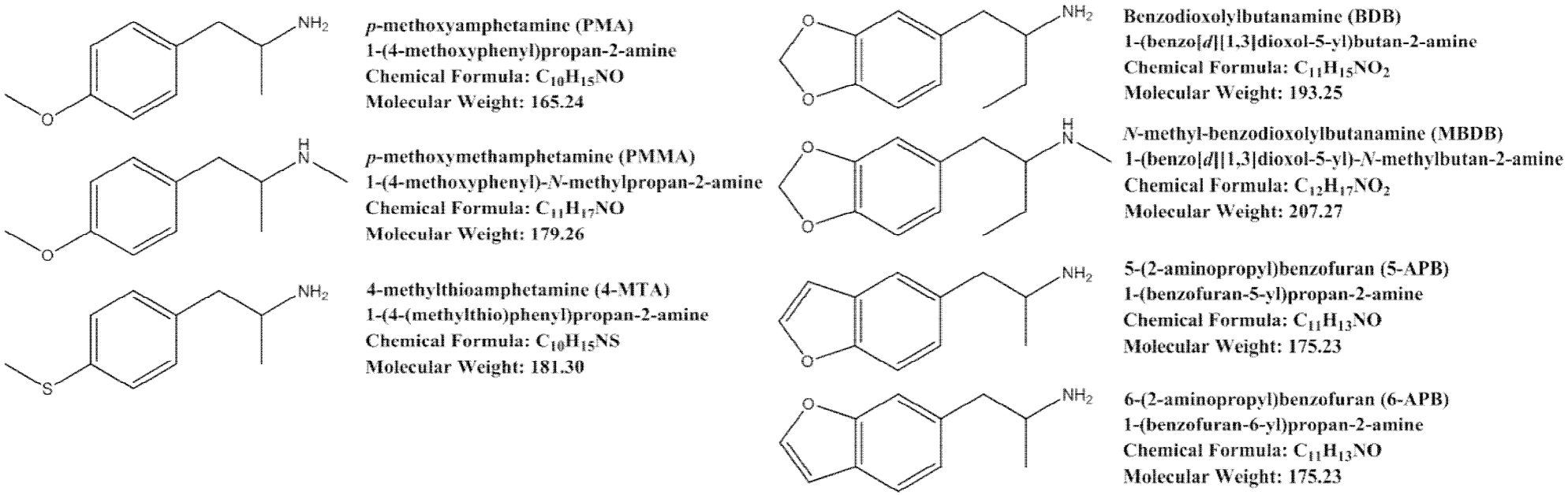

Figure 1: Seven phenethylamine-based designer drugs selected for this study.

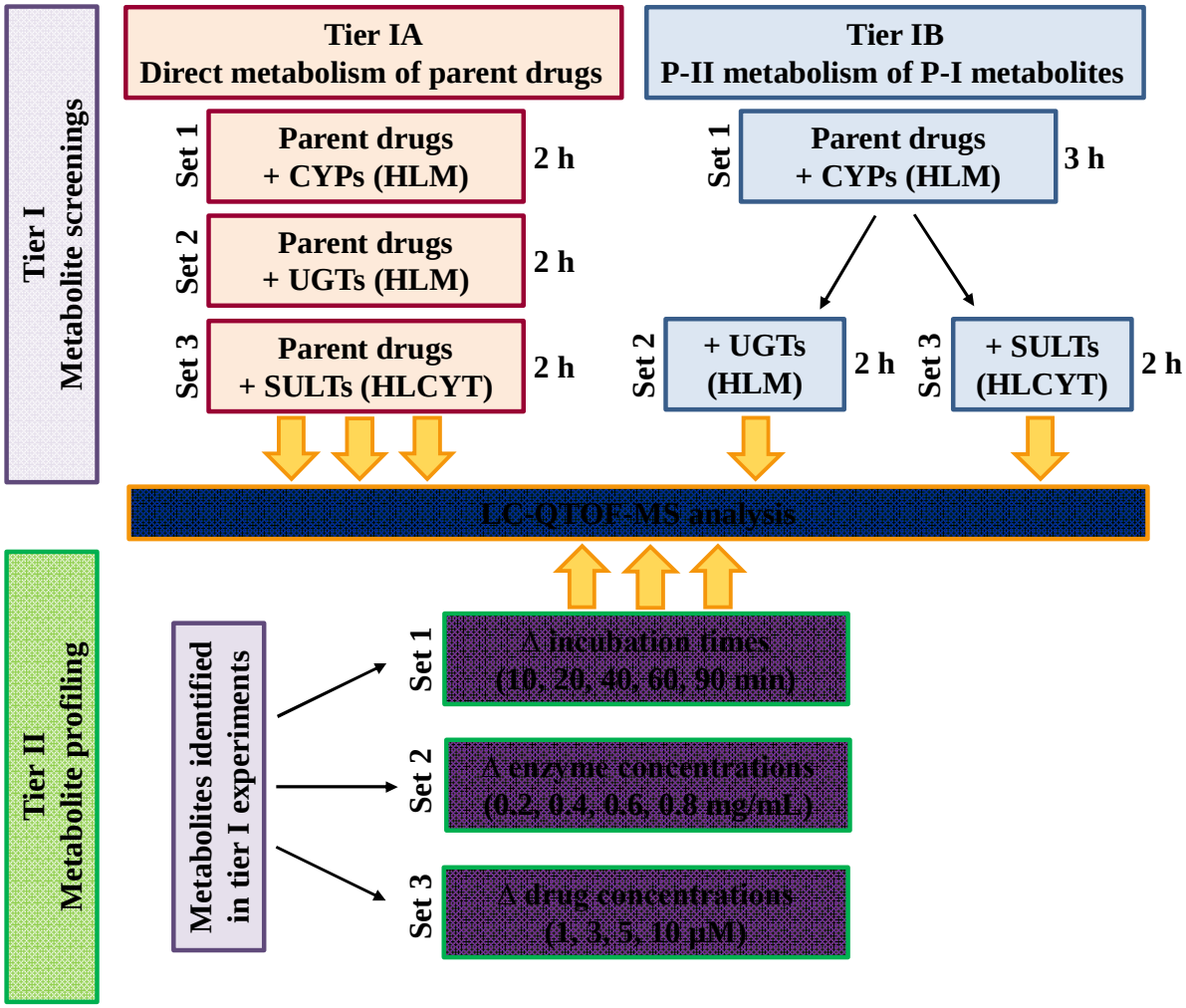

Figure 2: Schematic flow of the two-tiered approach on human *in vitro* drug metabolism.

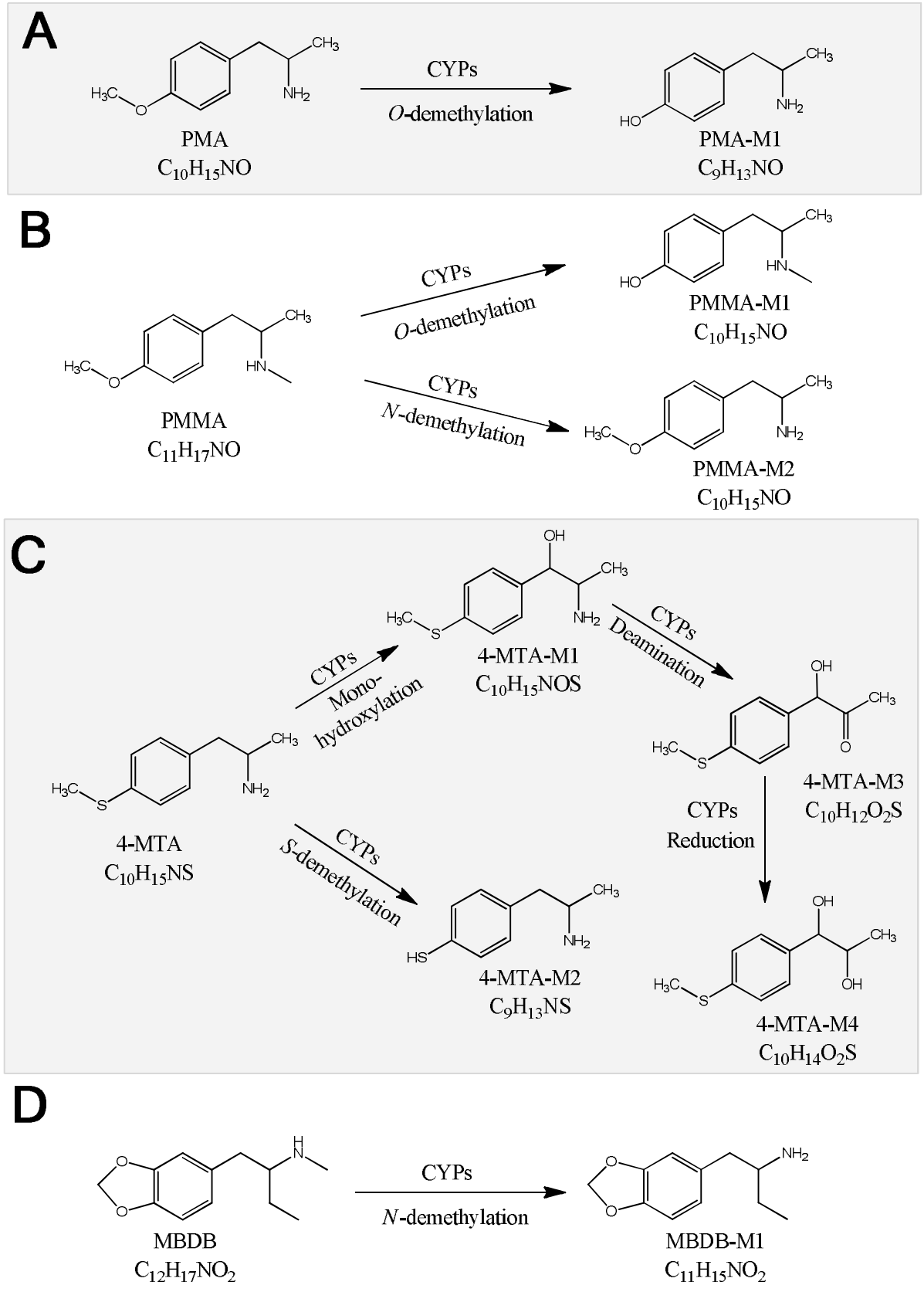

Figure 3: Proposed biotransformation pathways of PMA (**A**), PMMA (**B**), 4-MTA (**C**) and MBDB (**D**) by human CYP enzymes.

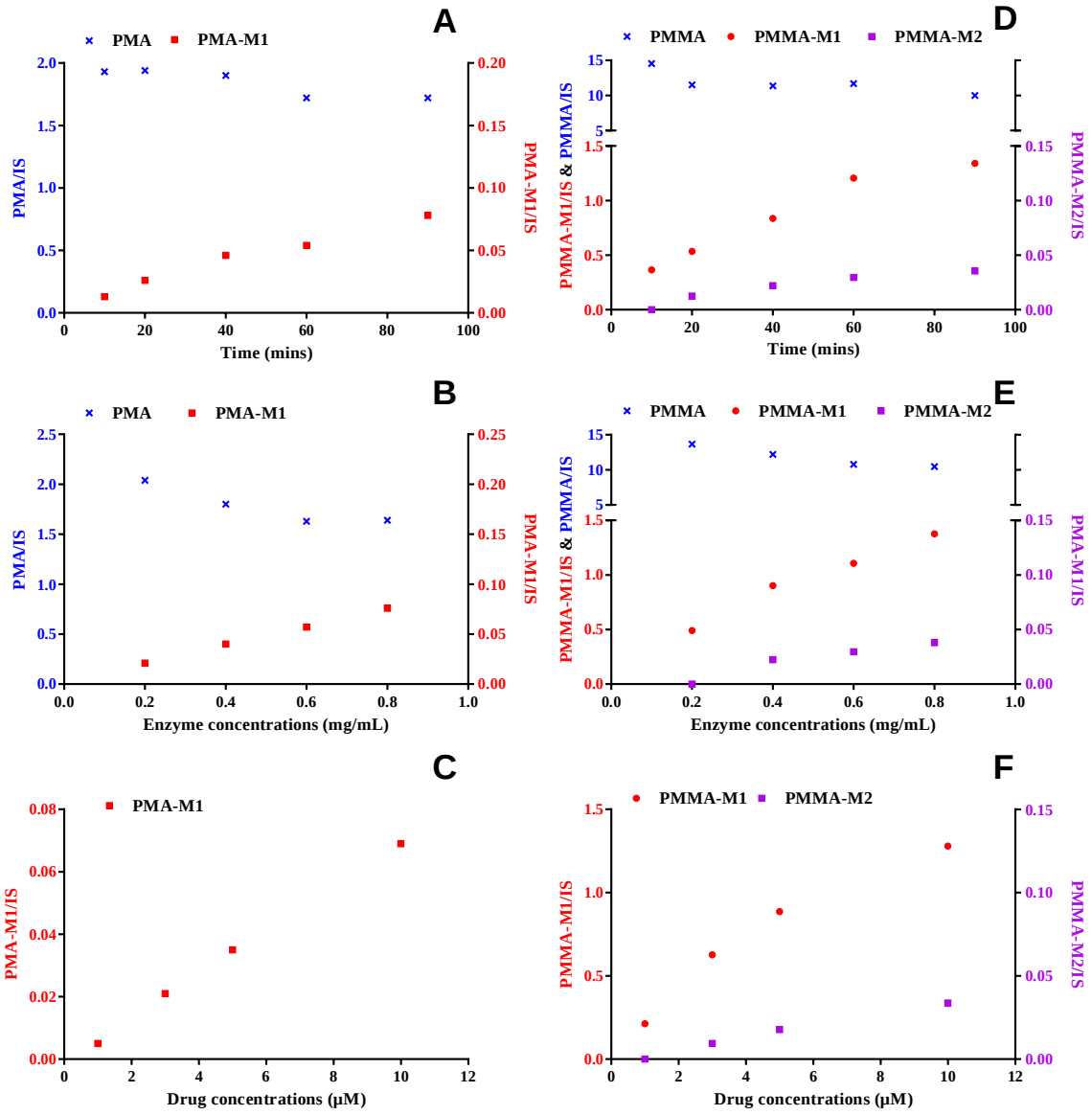

Figure 4: Metabolic profiles of PMA and its metabolite (**A–C**) and PMMA and its metabolites (**D–F**) under three different testing conditions (i.e. changes in the experimental times, enzyme concentrations and drug concentrations) in the tier II experiment. The response presents as the peak area ratio of the metabolites or parent drug to the internal standards. Note: when testing with the change in experimental times (i.e. A and D), the enzyme and substrate concentration was kept at 0.8 mg/mL and 10 μM, respectively; when testing with the change in the enzyme concentrations (i.e. B and E), the substrate concentration was kept at 10 μM and the experimental time was conducted for 90 min; when testing with the change in the substrate concentrations (i.e. C and F), the enzyme concentration was kept at 0.8 mg/mL and the experimental time was conducted for 90 min. See Tables 1 and 2 for the molecular structures of the metabolites.

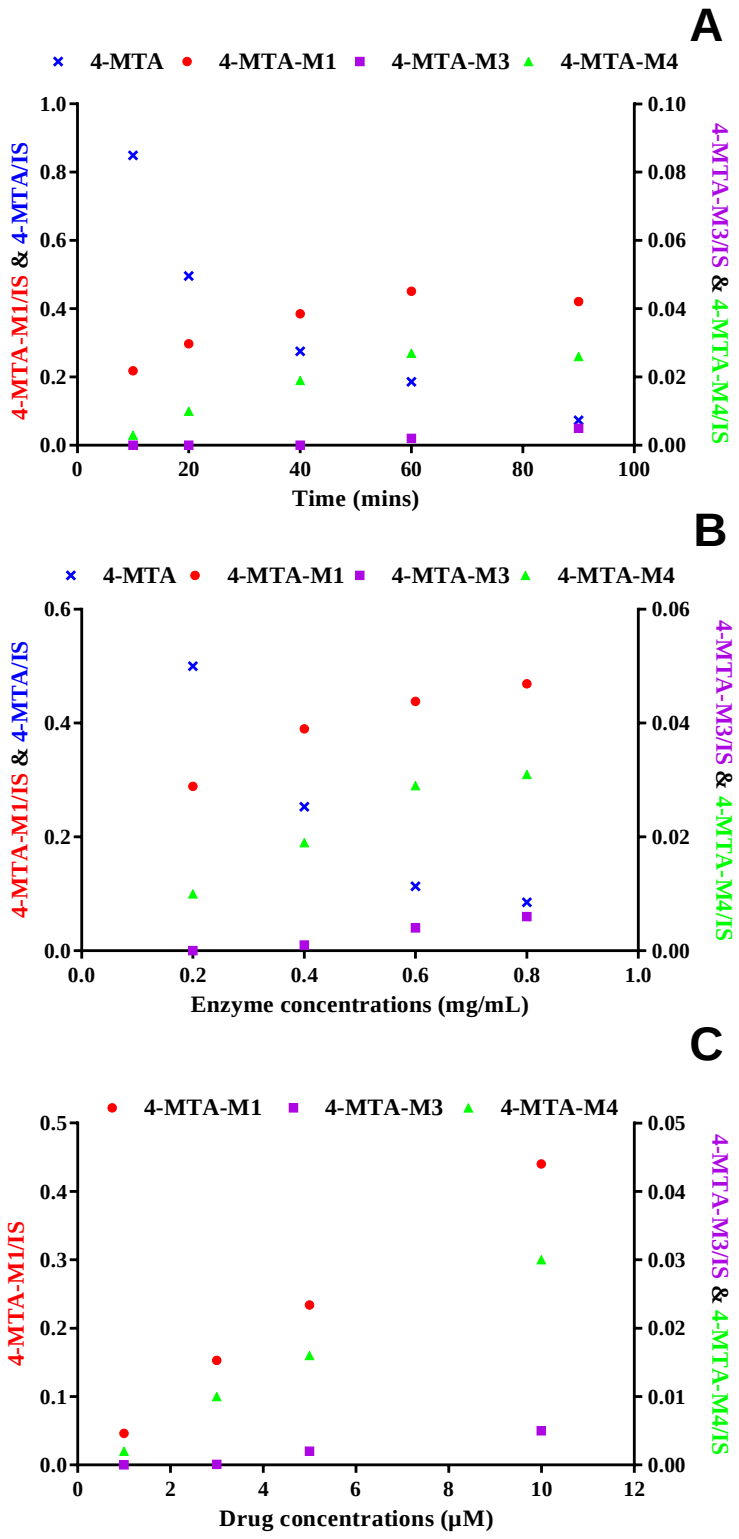

Figure 5: Metabolic profiles of 4-MTA and its metabolites under three different testing conditions (i.e. changes in the experimental times, enzyme concentrations and drug concentrations) in the tier II experiment. The response presents as the peak area ratio of the metabolites or parent drug to the internal standards. Note: when testing with the change in experimental times (i.e. A), the enzyme and substrate concentration was kept at 0.8 mg/mL and 10 μM, respectively; when testing with the change in the enzyme concentrations (i.e. B), the substrate concentration was kept at 10 μM and the experimental time was conducted for 90 min; when testing with the change in the substrate concentrations (i.e. C), the enzyme concentration was kept at 0.8 mg/mL and the experimental time was conducted for 90 min. See Table 3 for the molecular structures of the metabolites.

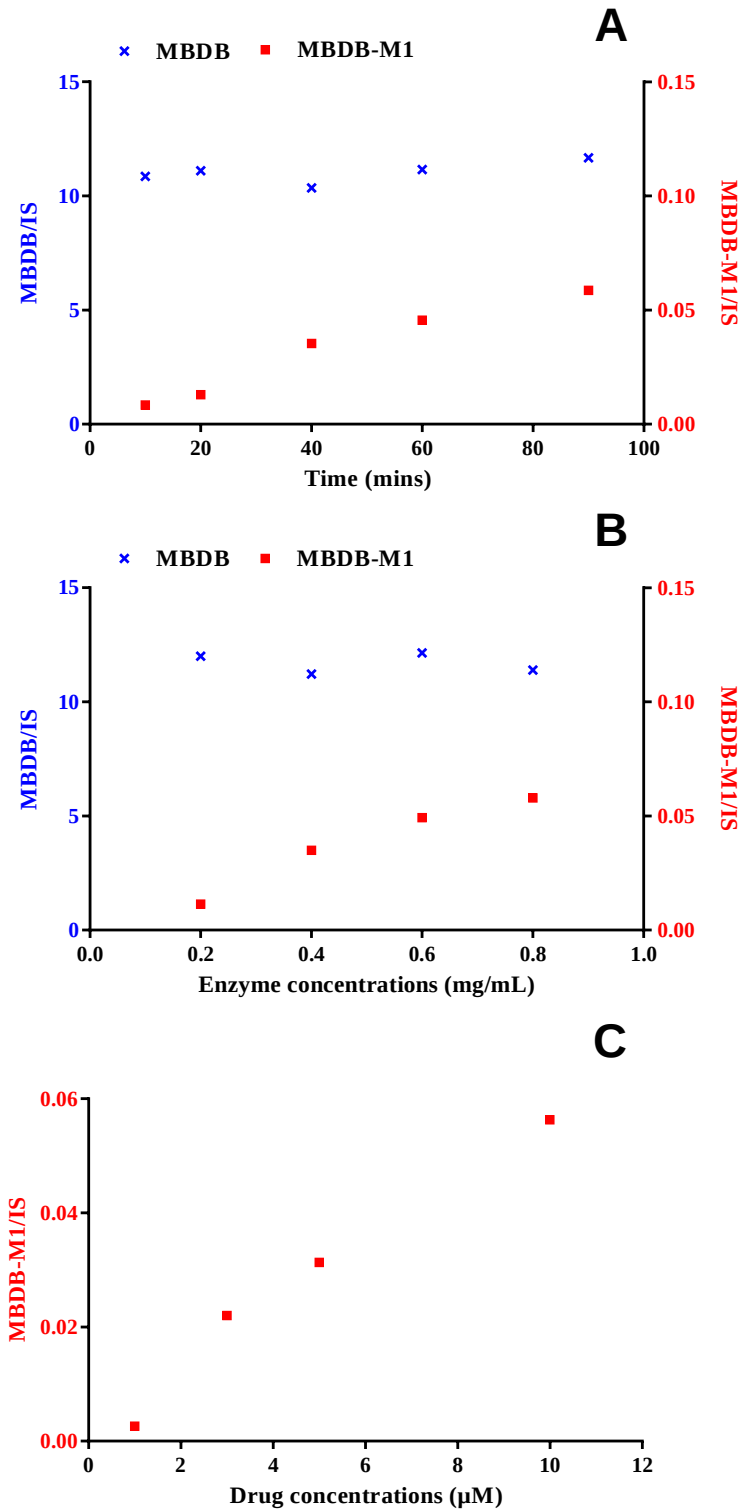

773

774 **Figure 6:** Metabolic profiles of MBDB and its metabolite under three different testing conditions (i.e. changes
775 in the experimental times, enzyme concentrations and drug concentrations) in the tier II experiment. The
776 response presents as the peak area ratio of the metabolites or parent drug to the internal standards. Note: when
777 testing with the change in experimental times (i.e. A), the enzyme and substrate concentration was kept at 0.8
778 mg/mL and 10 µM, respectively; when testing with the change in the enzyme concentrations (i.e. B), the
779 substrate concentration was kept at 10 µM and the experimental time was conducted for 90 min; when testing
780 with the change in the substrate concentrations (i.e. C), the enzyme concentration was kept at 0.8 mg/mL and
781 the experimental time was conducted for 90 min. See Table 4 for the molecular structure of the metabolite.